Photochemistry and Photobiology, 2016, 92: 826–834

Disinfection and Mechanistic Insights of *Escherichia coli* in Water by Bismuth Oxyhalide Photocatalysis

Ilana Sherman[1,2], Yoram Gerchman[3], Yoel Sasson[4], Hani Gnayem[4] and Hadas Mamane[1,2]*

[1]School of Mechanical Engineering, Tel Aviv University, Tel Aviv, Israel
[2]The Water Research Center at Tel-Aviv University, Tel Aviv, Israel
[3]Department of Biology and Environment, Faculty of Natural Sciences, University of Haifa, Oranim, Tivon, Israel
[4]Casali center of Applied Chemistry, The Institute of Chemistry, The Hebrew University of Jerusalem, Jerusalem, Israel

Received 12 March 2016, accepted 31 July 2016, DOI: 10.1111/php.12635

ABSTRACT

This study demonstrates the potential of a new $BiOCl_{0.875}Br_{0.125}$ photocatalyst to disinfect *Escherichia coli* in water under simulated solar irradiation. Photocatalytic efficiency was examined for different photocatalyst loadings, solar wavelengths, exposure times, photocatalyst concentration × contact time (Ct) concept and with the use of scavengers. To elucidate the inactivation mechanism, we examined DNA damage, membrane damage, lipid peroxidation and protein release. Both photolysis and photocatalysis were negligible under visible irradiation, but enhanced photocatalytic activity was observed under solar UVA ($\lambda > 320$ nm) and UVB ($\lambda > 280$ nm), with 1.5 and 3.6 log inactivation, respectively, after 40 min of irradiation. The log inactivation *vs* Ct curve for *E. coli* by UVA/$BiOCl_{0.875}Br_{0.125}$ was fairly linear, with Ct = 10 g L^{-1} × min, resulting in 2 log inactivation. Photocatalytic treatment led to membrane damage, but without lipid peroxidation. Accordingly, protein was released from the cells after UVA or UVA/$BiOCl_{0.875}Br_{0.125}$ treatment. Photocatalysis also increased endonuclease-sensitive sites *vs* photolysis alone, by an unknown mechanism. Finally, *E. coli* inactivation was not influenced by the addition of tert-butanol or L-histidine, implying that neither hydroxyl radicals nor singlet oxygen reactive species are involved in the inactivation process.

INTRODUCTION

Concerns about the formation of potentially carcinogenic disinfection byproducts have led to the development of alternative processes for the disinfection of drinking water. In this context, novel treatment methods based on photodisinfection hold very promising potential to provide safe drinking water, using solar energy as a green and sustainable energy source. Photocatalytic disinfection involves three components that are individually harmless to the biological environment, specifically the photosensitizer, light and molecular oxygen. The term photosensitizers, however, generally refers to organic catalyst (as methylene blue, rhodamine B and porphyrins) whereas the term photocatalyst refers to inorganic catalysts (as titanium dioxide (TiO_2), zinc oxide (ZnO), ferric oxide (Fe_2O_3)) (1).

To date, the most common photocatalysts are based on titanium dioxide (TiO_2) (2–4), but there is great interest in others, among them those based on bismuth. Bismuth-based photocatalysts are excellent candidates for solar light-driven processes, due to their possible visible and UVA light absorbance and their nontoxic nature (5). For example, the photocatalysts Bi_2WO_6, $CaBi_2O_4$ and $NaBiO_3$ were found to be efficient for degradation of rhodamine B, bisphenol A, dyes and other organic pollutants under simulated solar irradiation and UV light (3,6–8). However, most of the research has focused on the photocatalytic degradation of organic pollutants, with limited studies investigating the photocatalytic inactivation of microorganisms (9–11). Shenawi-Khalil *et al.* (12) were the first to demonstrate the photoreactivity of a new family of bismuth-mixed oxyhalide photocatalysts with the general structure of $BiOCl_{1-x}Br_x$ ($0 \leq x \leq 1$). The photocatalyst with $x = 0.5$ exhibited higher reactivity than Degussa P25 in removing the dye molecule rhodamine B, using similar photocatalyst concentrations, under both UV–visible ($\lambda \geq 385$ nm) and visible light ($\lambda \geq 420$ nm). Gnayem and Sasson (13) optimized the synthesis of the $BiOCl_{1-x}Br_x$ photocatalyst (with $x > 0.87$), resulting in a more effectual photocatalyst with unique morphologies and exceptional activity.

Photocatalysts are believed to affect cells by generating reactive oxygen species (ROS), especially hydroxyl radicals (HO•) (14). These ROS can result in lipid peroxidation, and damage to membrane integrity, DNA and proteins, subsequently leading to cell death (15). Lipid peroxidation, that is the conversion of unsaturated lipids to polar lipid hydroperoxides, results in decreased membrane fluidity and alters membrane properties (16). Solar radiation can also cause cellular DNA damage via two possible mechanisms: (1) direct excitation of DNA and (2) indirect mechanisms that involve the excitation of other cellular chromophores [endogenous photosensitizers, production of intercellular ROS (17–19)]. Direct excitation of DNA by short UV radiation (UVC, UVB) generates pyrimidine dimers which result directly in cell death (20,21). Indirect mechanisms are responsible for DNA damage at longer wavelengths (UVA, visible light), where DNA absorbs only weakly, if at all (17), although UVA can cause pyrimidine dimer formation and eventually, DNA lesions by ROS generated in the presence of oxygen (22,23). Another indirect mechanism may involve generation of endogenous (HO•) via superoxide anions (O_2^-) and the Fenton reaction (24).

*Corresponding author e-mail: hadasmg@tauex.tau.ac.il (Hadas Mamane)

In addition to membrane lipid and DNA damage, proteins are major biological targets for ROS. Protein oxidation is known to be a key factor in cellular aging in eukaryotes. The tertiary structure of oxidized proteins is thermodynamically unstable and, therefore, oxidized proteins tend to expose hydrophobic amino acids to the outside, with consequential agglutination and cross-linking (25). At the cellular level, when proteins are exposed to ROS, amino acid side chains are modified and, consequently, the protein structure is altered. These modifications lead to functional changes that disrupt cellular metabolism (16).

To date, there have been no reports on the mechanism governing the inactivation of *Escherichia coli* by $BiOCl_{1-x}Br_x$ photocatalyst. This study demonstrates the potential of a new heterojunctioned $BiOCl_{0.875}Br_{0.125}$ photocatalyst to disinfect *E. coli* in water under simulated solar irradiation with different photocatalyst loadings, solar wavelengths, exposure times and the use of scavengers. The inactivation mechanism was deciphered in terms of membrane damage, DNA damage, lipid peroxidation and protein release.

MATERIALS AND METHODS

Preparation and characterization of $BiOCl_xBr_{1-x}$ (x = 0.875) photocatalyst. The catalyst was developed and synthesized and characterized as described in Gnayem and Sasson (13). Morphological observations were made with a high-resolution scanning electron microscope (HRSEM) Sirion (equipped with EDS LN2 detector, Oxford instruments, UK) and with transmission electron microscope (TEM) (Philips, CM-120, 120 kV) (Fig. 1a,b, respectively). At low magnification, the typical TEM image shows several microspheres, constructed from very thin nanoplates, connected densely to each other to form flower-like structures, confirming the 3D flower-like surface microstructure already revealed by HRSEM. The particle size was measured using a Malvern Instruments Mastersizer 2000 particle size analyzer (Fig. 2).

Preparation of aqueous suspensions of $BiOCl_{0.875}Br_{0.125}$. Bismuth powder (7.5 mg) was added to 1 mL of 0.9% (w/v) NaCl in an Eppendorf tube and sonicated for 15–20 min to create a homogeneous, aggregate-free suspension. The bismuth was then mixed with 29 mL of *E. coli* suspension as detailed below.

Preparation of microorganism. Escherichia coli K-12 (ATCC 23631) was used as the test bacterium. A single colony was inoculated into 5 mL sterile liquid tryptone broth and incubated overnight (15–18 h) at 37°C and then transferred into a 250 mL Erlenmeyer flask containing 45 mL liquid tryptone and shaken at 37°C, 125 rpm to obtain an exponential-phase culture with OD_{540} of ~0.7. The suspension was centrifuged at 4000 ***g*** at room temperature for 10 min and the bacterial pellet was washed twice in deionized (DI) water. The pellet was then resuspended in 0.9% NaCl to a final concentration of ~10^7 CFU mL^{-1}.

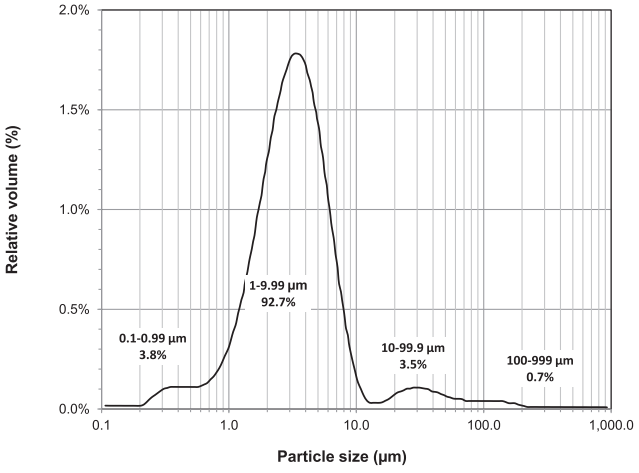

Figure 1. Particle size distribution of $BiOCl_{0.875}Br_{0.125}$ photocatalyst.

Experimental procedure for inactivation experiments. A 150W ozone-free xenon arc lamp (Sciencetech Inc., SS150W, Canada) was used with a maximum optical output irradiance given by the manufacturer of 1000 W m^{-2}, after the light beam was filtered through a 1.5 global air mass filter. In reality, other losses in our laboratory system and design around the target resulted in irradiance of ~800 W m^{-2}. This simulator is defined as class AAA performance American Society for Testing and Materials (ASTM E927) standards, meaning that three parameters are required: spectral match, nonuniformity of irradiance less than ±2% and temporal instability less than ±2%. The output spectrum of the solar simulator would be equivalent to natural sunlight at 48.2° latitude at sea level. The solar simulator setup, calibration and spectrum were as previously described (26,27). Incident irradiance values of solar simulator was measured via a spectro-radiometer (International light, ILT 900R). Comparison of spectra obtained from the solar simulator with 1.5G filter and the natural sun was previously published (26). Results showed that although the spectral match under 400 nm is not part of the ASTM standard, examination on a randomly chosen mid-summer day (at 12:00 noon) gave a spectrum similar to that achieved by the simulator (especially below 400 nm).

To obtain dose–response curves, *E. coli* suspensions were irradiated. Samples (10 mL) of *E. coli* K-12 in 0.9% NaCl at a concentration of ~10^7 CFU mL^{-1} with 0.25 g L^{-1} bismuth photocatalyst (prepared as above) were placed under the solar simulator light. The samples were irradiated in a 50 mm diameter × 35 mm height Pyrex dish under continuous stirring. Two long-pass (LP) filters (320 LP and 280 LP, which screened all light below 280 and 320 nm, respectively; Fig. 3) were adjusted at approximately 2 cm above the vessel. Subsamples of 0.1 mL were taken at predetermined times for further analysis. The dishes were wrapped with a hollow copper tube connected to a chiller (BL-30, MRC, Israel) for circulating water at the desired temperature. Water temperature was measured inside the Pyrex dish by a thermocouple and kept under ~35°C.

Enumeration of the bacterium. To evaluate inactivation of the bacterial suspension, samples were taken at designated times during the experiments. Serial dilutions were performed in sterile phosphate buffer saline (PBS), and viable *E. coli* were enumerated by spreading 0.1 mL on mFC selective agar (HiMedia, India). The dishes were incubated overnight at 37°C and colonies were counted the following day. In every experiment, two replicate plates were used for each exposure times. Three independent experiments were conducted for each condition. For each treatment, at various time points, the mean of the test microorganism (from at least three separate experiments) was calculated and taken as N_t. The $\log_{10}$ inactivation for N_t/N_0 for *E. coli* was plotted as a function of the exposure time.

Endonuclease-sensitive site assay. The endonuclease-sensitive site (ESS) assay was used to obtain a quantitative evaluation of DNA damage in *E. coli* exposed to irradiation. To obtain a sufficient amount of DNA, a higher concentration of *E. coli* was used in 0.9% NaCl for ESS assays (~10^8 CFU mL^{-1}) than for the inactivation experiments (10^7 CFU mL^{-1}). Cells were harvested by centrifugation and genomic DNA was isolated using a commercial kit (QIAamp DNA Mini Kit) (26). *E. coli* DNA absorbance is presented in Supporting Information Fig. S1 and Data S1.

Lipid peroxidation. Lipid peroxidation level was measured by quantifying malondialdehyde (MDA) using a commercial kit (TBARS Assay Kit). A predetermined concentration of 1 µM MDA standard from the TBARS assay kit was added to 10 mL of 0.9% NaCl solution and irradiated under UVA and longer wavelengths (with the 320 LP filter) for different periods of time, in the presence or absence of 0.25 g L^{-1} bismuth photocatalyst. The fluorescence was read at an excitation wavelength of 530 nm and emission wavelength of 550 nm using an FL3-11 spectrofluorometer (Horiba).

Protein release from cells. Protein was quantified in the bulk liquid, after removal of bacteria, by centrifugation (5 min, 10 000 ***g***, room temperature) using the Quick Start Bradford Protein Assay Kit (Bio-Rad Laboratories). Protein concentration was calculated by measuring absorbance in a spectrophotometer. An effort was made to correct for the bismuth effect on the assay (see Data S2, Fig. S2).

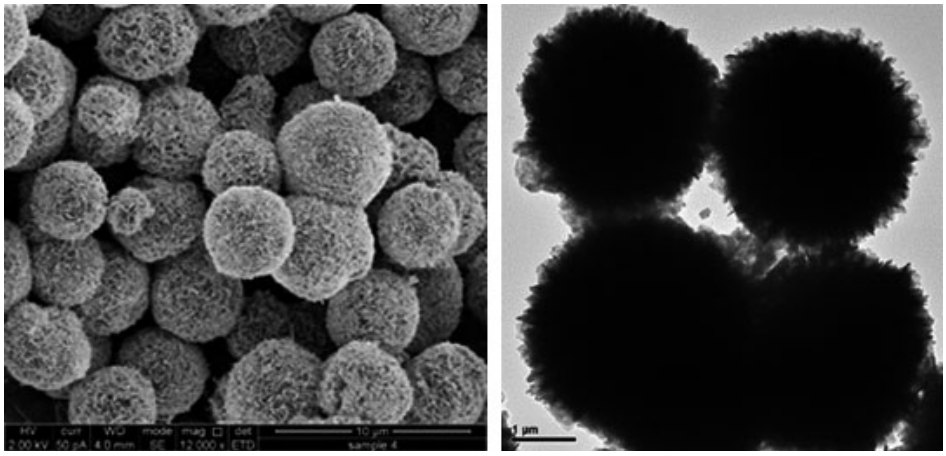

Figure 2. SEM (left) and TEM (right) micrographs of $BiOCl_{0.875}Br_{0.125}$ photocatalyst.

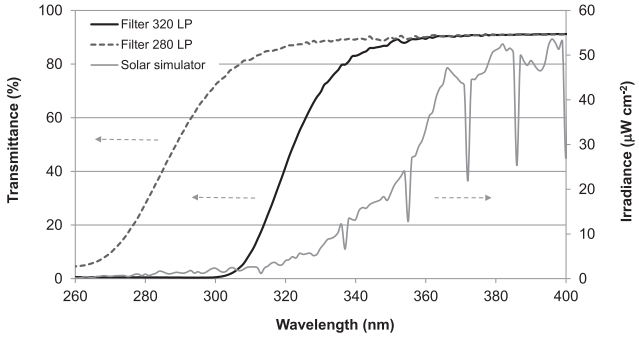

Figure 3. Solar simulator incident irradiation and transmittance for the selected filters as a function of wavelength.

Live/Dead BacLight bacterial viability assay. The Live/Dead BacLight Bacterial Viability Kit is routinely used to detect the efficacy of bactericidal agents (Invitrogen–Molecular Probes). The initial *E. coli* concentration was ~10^8 CFU mL^{-1} in 0.9% NaCl. A 3 mL aliquot of the treated sample was centrifuged at 10 900 ***g*** for 10 min and the pellet was resuspended in 997 μL of 0.9% NaCl. The bacterial suspensions were stained with 2 μL propidium iodide (PI) and 1 μL SYTO-9 dye and kept in the dark at room temperature for 30 min. The suspensions were then centrifuged, the pellet was smeared on a glass microslide (X-tra Adhesive, Surgipath) and 15 μL of antifading solution (sodium thiosulfate solution, 0.1 mol L^{-1}, Fluka Analytical, Sigma-Aldrich) was added; this was covered with a microscope coverslip (VWR International). The slides were viewed using a Zeiss LSM-510 confocal microscope. The images were captured from four randomly selected areas and saved as TIFF files. For each sample, 15 fields of view were taken with a field size of 164 × 164 μm.

Radical scavengers. Stock solutions of tert-butanol and L-histidine (Sigma-Aldrich) were prepared in DI at a concentration of 0.5 M. The scavengers were added separately to *E. coli* in 0.9% NaCl (initial concentration ~10^7 CFU mL^{-1}). The final concentration of tert-butanol and L-histidine was 30 mM. The suspension was thoroughly mixed and kept in the dark for 15 min and then irradiated with 0.25 g L^{-1} photocatalyst under $\lambda > 280$ nm light (280 LP filter, under the solar simulator).

RESULTS AND DISCUSSION

Bismuth oxyhalide particle size and size distribution

The size distribution of the bismuth particles is relatively narrow (i.e. mostly between 1 and 10 μm, with $d_{0.5}$ of 3.2 μm) (Figs 1 and 2). This places the particles in the same size scale and even larger than the *E. coli* cells (typically less than 1 μm wide) making penetration into the cells very unlikely, and suggesting that the photocatalytic action occurred externally to the bacterial cell. This idea is supported by the work of Adán *et al.* (28) that studied the photocatalytic oxidation of small molecule (methanol) and the inactivation of *E. coli* by bismuth vanadates ($BiVO_4$) particles of similar size (2–10 μm size), and concluded that while the internal surfaces were available for the methanol only the most external surface of the $BiVO_4$ particles was available for the interaction with the bacteria. To conclude, it is very unlikely that bismuth oxyhalide particles could enter the cell, and its interaction is probably limited to the bismuth external surface.

Effects of UVA and UVB on *E. coli* inactivation

UV radiation is usually classified into three wavelength ranges: UVA (320–400 nm), UVB (280–320 nm) and UVC (<280 nm). Most of the UV radiation reaching the earth's surface is UVA (~99%), as the atmospheric ozone layer absorbs UVC and most of the UVB. The solar simulator used in this study was comparable to the natural spectrum from sunlight exposure. The effects of UVA, UVB and visible light on *E. coli* inactivation were examined using two LP filters, for examined wavelength ranges of $\lambda > 280$ nm (280 LP) and $\lambda > 320$ nm (320 LP). The incident irradiance values of the solar simulator for UVA wavelengths only (320–400 nm) were 23.83 W m^{-2} and ~5% of the measured solar spectrum (400–950 nm). The solar simulator's incident irradiation and transmittance for the selected filters as a function of wavelength are given in Fig. 3.

Figure 4 illustrates the log inactivation of *E. coli* by light filtered through the 280 LP and 320 LP filters as a function of irradiation time in the presence or absence of 0.25 g L^{-1} bismuth photocatalyst. Suspensions of *E. coli* at a concentration of ~10^7 CFU mL^{-1} in 0.9% NaCl were irradiated for 80 min and samples were taken at different time points.

Direct photolysis of *E. coli* after 80 min of exposure under UVA and longer wavelengths ($\lambda > 320$ nm) in the solar simulator was marginal (0.96 ± 0.31 log); however, direct photolysis under UVB and longer wavelengths ($\lambda > 280$ nm) was substantial (4.5 ± 0.36 log). In the wavelength range of the solar simulator, only the UVB (280–320 nm) region overlapped with the

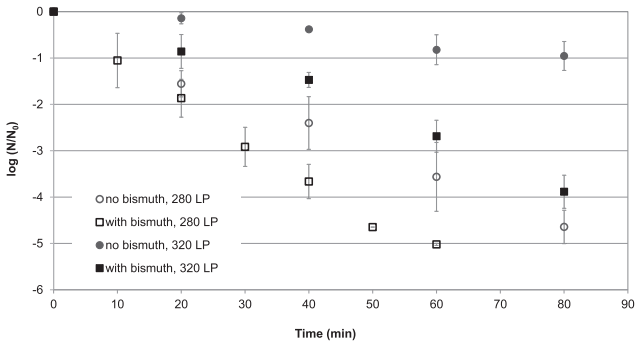

Figure 4. Inactivation of *E. coli* by UVA ($\lambda > 320$ nm) and UVB ($\lambda > 280$ nm) spectral irradiation in the presence (with bismuth) or absence (no bismuth) of 0.25 g L^{-1} photocatalyst. Log N/N_0 values as a function of irradiation time. Initial *E. coli* concentration ~2 × 10^7 CFU mL^{-1}.

tail of DNA absorbance (see Fig. S1). Therefore, it is at those wavelengths that *E. coli* DNA will be most affected by UVB irradiation. UVB radiation is a minor part of the solar spectrum; however, it has a disproportionate effect on bacterial inactivation (18), as observed in this study. Similar photolytic inactivation results have been presented (26,29), demonstrating inactivation of ~5 log of *E. coli* after 90 min of natural solar irradiation.

Addition of 0.25 g L^{-1} bismuth photocatalyst produced a significantly larger difference in *E. coli* inactivation under UVA *vs* UVB, compared with samples without bismuth exposed to the same wavelengths and doses. Photolytic and photocatalytic inactivation of *E. coli* with 0.25 g L^{-1} bismuth by UVA ($\lambda > 320$ nm) followed first-order kinetics with rate constants (k) of 1.2 × 10^{-2} min^{-1} and 4.5 × 10^{-2} min^{-1}, respectively, and by UVB ($\lambda > 280$ nm) with rate constants of 5.94 × 10^{-2} min^{-1} and 9.3 × 10^{-2} min^{-1}, respectively. Under UVA and UVB, the rate constants of a photocatalytic reaction were 3- and 1.5-fold greater than the photolytic constant, respectively. In the literature, the rate constants of *E. coli* inactivation when exposed to UVA/TiO_2 were 3.7 × 10^{-1} min^{-1} (2 g L^{-1} TiO_2) and 2.9 × 10^{-1} min^{-1} (0.1 g L^{-1} TiO_2) (30,31). However, a comparison between the rate constants may not be valid, due to different ROS, photocatalyst types and concentrations, and light sources.

The dependence of photolysis and photocatalysis on wavelength is best understood by the contribution of each spectral range to the total inactivation of *E. coli*. With the addition of 0.25 g L^{-1} bismuth, 3.88 ± 0.35 log inactivation was observed after 80 min of irradiation with the 320 LP filter. Similar results were achieved after only 40 min of irradiation with the 280 LP filter. When a photocatalytic process consists mainly of UVA, the inactivation mechanism is attributed to a photo-oxidative process as well as to the generation of ROS (32). Thus, photocatalysis of *E. coli* in the presence of bismuth under the solar simulator showed that this bacterium is susceptible to inactivation mechanisms additional to direct photolysis.

Bismuth-based inactivation in visible light ($\lambda > 400$ nm) has been previously reported (Table 1). Nevertheless, in the current study, the bismuth photocatalyst was not bactericidal under visible light (a 400 LP filter resulted in less than 1 log reduction after 80 min of irradiation). This negligible inactivation of *E. coli* under visible light may be the most realistic outcome, in view of the varying results with previous studies for bismuth-based formulations (Table 1). Our results also agree well with those published by Lester *et al.* (27) showing that the $BiOCl_{0.875}Br_{0.125}$ formulation does not absorb light at wavelengths longer than ~380 nm, resulting in only minor carbamazepine removal under visible light alone ($\lambda > 400$ nm).

Disinfection kinetics

The effectiveness of the disinfection process can be expressed as the product Ct, where C is the disinfectant concentration (expressed in mg L^{-1}) and t is the contact time (expressed in min) needed to inactivate a determined percentage of the pathogen's population (14). The simplest disinfection model (Eq. 1) is a combined one proposed by Chick (33,34) and Watson (33,34). In the Chick–Watson model, the rate of inactivation of a microorganism is dependent upon the (residual) concentration of the disinfectant and contact time. In Eq. (1), N/N_0 is the reduction in the concentration of the microorganism; k is the disinfection kinetics constant, C was taken as the concentration of $BiOCl_{0.875}Br_{0.125}$ (g L^{-1}), n is the reaction order and t is the irradiation time (min). The n value for the Chick–Watson law is close to 1.0 and hence a fixed value of the product of residual concentration and time (Ct product) results in a fixed degree of inactivation. Effective disinfectant requires maintenance of a specified concentration of disinfectant and contact time, to achieve the target value of Ct, and is valuable for comparing the disinfection effectiveness of disinfectants. For a given microorganism, low Ct values represent an effective disinfectant and vice versa. For different microorganisms, Ct values allow to compare the sensitivity of different organisms to the same disinfectant. In addition, the Ct concept allows the calculation of concentration (at a given contact time) or contact time (at a given disinfectant concentration) to obtain a required log inactivation.

$$\log\left(\frac{N}{N_0}\right) = -kC^n t = -k \times Ct \qquad (1)$$

In the case of conventional disinfection, the Ct values for achieving 1 log inactivation of *E. coli* were 0.085 mg L^{-1} × min, 0.0021 mg L^{-1} × min and 0.030 mg L^{-1} × min for free chlorine, ozone and chlorine dioxide, as the residual disinfectant concentration (C), respectively (23). However, when referring to photocatalytic disinfection, Ct may be defined differently. For example, Cho *et al.* (35) calculated Ct for inactivation of *E. coli* under UV/TiO_2, where C is the concentration of HO•, as the primary oxidant species responsible for *E. coli* inactivation. They found a Ct value of 0.8 × 10^{-5} mg L^{-1} × min for achieving 2 log inactivation of *E. coli*, as predicted by the delayed Chick–Watson model. The Ct values reported in the literature for other disinfectants, such as UV/H_2O_2 (18,35), were 1.5 × 10^{-8} g L^{-1} × min and 4.9 × 10^{-9} g L^{-1} × min, several magnitudes lower than those presented here. However, in those cases, the C was defined as the concentration of HO•, and therefore, the results cannot be compared.

To investigate the linearity of the photocatalyst, C was taken as the concentration of $BiOCl_{0.875}Br_{0.125}$ (g L^{-1}), and not that of the major oxidative species as suggested in the previous studies, and t as irradiation time (min). Figure 5 illustrates the inactivation of *E. coli* by UVA/$BiOCl_{0.875}Br_{0.125}$ ($\lambda > 320$ nm using the

Table 1. Literature review of bismuth-based photocatalytic inactivation of microorganisms.

Bismuth photocatalyst	Photocatalyst concentration	Microorganism	Exposure time	λ (nm)	Initial (CFU mL^{-1})	Log inactivation	Author
Bi_2WO_6	500 mg L^{-1}	*Escherichia coli*	2 h	>420	~2×10^7	0.02	Ren *et al.* (9)
$BiVO_4$	100 mg L^{-1}	*E. coli* K-12	5 h	>400	~2×10^5	4	Wang *et al.* (11)
AgBr-Ag-Bi_2WO_6	100 mg L^{-1}	*E. coli* K-12	15 min	>400	~5×10^7	7	Zhang *et al.* (10)
$BiCO/BiNbO^{-2}$	1 g L^{-1}	*E. coli*	5 h	>400	~1×10^5	4.7	Gan *et al.* (50)
$BiVO_4$	500 mg L^{-1}	*E. coli* K-12	4 h	>380	~1×10^6	4	Adán *et al.* (28)

320 LP filter) for different Ct products. A fairly linear disinfection profile was obtained; the calculated k value was 0.199 g^{-1} $min^{-1} \times L$ with $R^2 = 0.89$. The photocatalyst Ct required to achieve 2 log inactivation of *E. coli* was 10 g $L^{-1} \times$ min. Nevertheless, in the case of Ct for photocatalysis, there are many factors to be considered, such as the UV irradiation dose and wavelengths, and the different ROS mechanisms, which are not discussed herein.

Mechanism of inactivation

Possible mechanisms of microbial inactivation were investigated by examining changes in cell wall permeability, quantifying pyrimidine dimers, evaluating lipid peroxidation and the amount of protein oxidized, and by determining the effect of ROS scavengers on inactivation.

Membrane damage—live/dead assay

Membrane damage was examined after catalytic and photocatalytic treatment with 0.25 g L^{-1} bismuth at $\lambda > 320$ nm (320 LP filter) under the solar simulator. The fluorescent dyes used in the assay were SYTO-9, which labels all bacteria (fluoresces green), and PI which penetrates only bacteria with compromised membranes (fluoresces red). Figure 6 illustrates the changes in cell permeability during the treatment. Without particle addition, almost all cells stained green (Fig. 6a) and were viable, as determined by plating assay. Addition of bismuth oxyhalide particles (without irradiation) resulted in some immediate catalytic damage (Fig. 6b) that became more evident as irradiation time accumulated, as demonstrated by the increase in the amount of red fluorescing cells (Fig. 6c–d). Accordingly, when cells treated for 40 min were plated, only 3%, as compared to the pretreated cells, were able to form colonies. These results and the rapid effect of the photocatalyst suggested that the combination of UVA and $BiOCl_{0.875}Br_{0.125}$ damages bacterial membrane permeability, eventually leading to cell death. These results were in agreement with those reported for UVA/TiO_2 treatment (36).

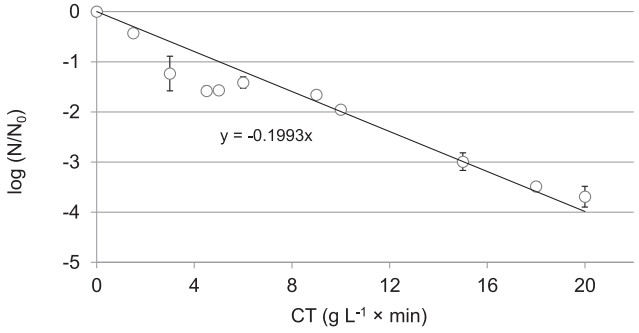

Figure 5. Ct-based inactivation of *E. coli* at different bismuth concentrations under UVA light exposure ($\lambda > 320$ nm), where C is the concentration of bismuth and t is the irradiation time. Log N/N_0 values as a function of Ct (g $L^{-1} \times$ min). Initial *E. coli* concentration ~2×10^7 CFU mL^{-1}.

Although informative, there are certain limitations to the use of PI and SYTO-9 staining for characterization of bacterial viability in the presence of a suspended photocatalyst, as such particles could adsorb the fluorescent dyes, resulting in false-positive results. Pigeot-Rémy *et al.* (36) and Josset *et al.* (37) mentioned this issue using TiO_2 nanoparticles, and absorption to the dyes was clearly evident for the bismuth oxyhalide particles, even at time 0 (Fig. 6b). In our case, the adsorption probably occurred due to the opposing charges of the bismuth particles (negative at pH 5.5~6; Gnayem and Sasson (13)) *vs* the PI stain positive charge.

Furthermore, Pigeot-Rémy *et al.* (36) noticed that in fluorescence microscopy images of UVA/TiO_2-treated *E. coli*, the bacterial cells were grouped together into small aggregates, suggesting that the contact between TiO_2 nanoparticles and bacterial cells induces the formation of aggregates, which further complicates enumeration. Given these limits, accurate enumeration was not achievable although clear differences can be seen (Fig. 6a–d).

Lipid peroxidation

Membrane damage by TiO_2 has often been associated with lipid peroxidation (38). This was analyzed by quantifying MDA, a product of lipid peroxidation, by TBARS assay (19,36,39,40). To avoid falsified results, experiments were conducted to validate the compatibility of the assay and examine the effect of photolysis and photocatalysis on MDA standards. MDA has been proposed to be a target of oxidative degradation as well, a process that could lead to underestimation of lipid peroxidation (39–41). Nevertheless, our experiments showed no MDA degradation during 40 min of either photolysis or $BiOCl_{0.875}Br_{0.125}$ photocatalytic treatments (data not shown). Thus, the assay was assumed to be reliable and the effects of UVA and UVA/$BiOCl_{0.875}Br_{0.125}$ on *E. coli* lipid peroxidation were tested. Neither photolysis (320 LP filter under the solar simulator for up to 40 min) nor photocatalysis (same, but in the presence of 0.25 g L^{-1} photocatalyst) of *E. coli* suspensions in 0.9% NaCl demonstrated any change in MDA concentration. Interestingly, with TiO_2 photocatalysis, MDA formation was observed from the beginning of the treatment (36).

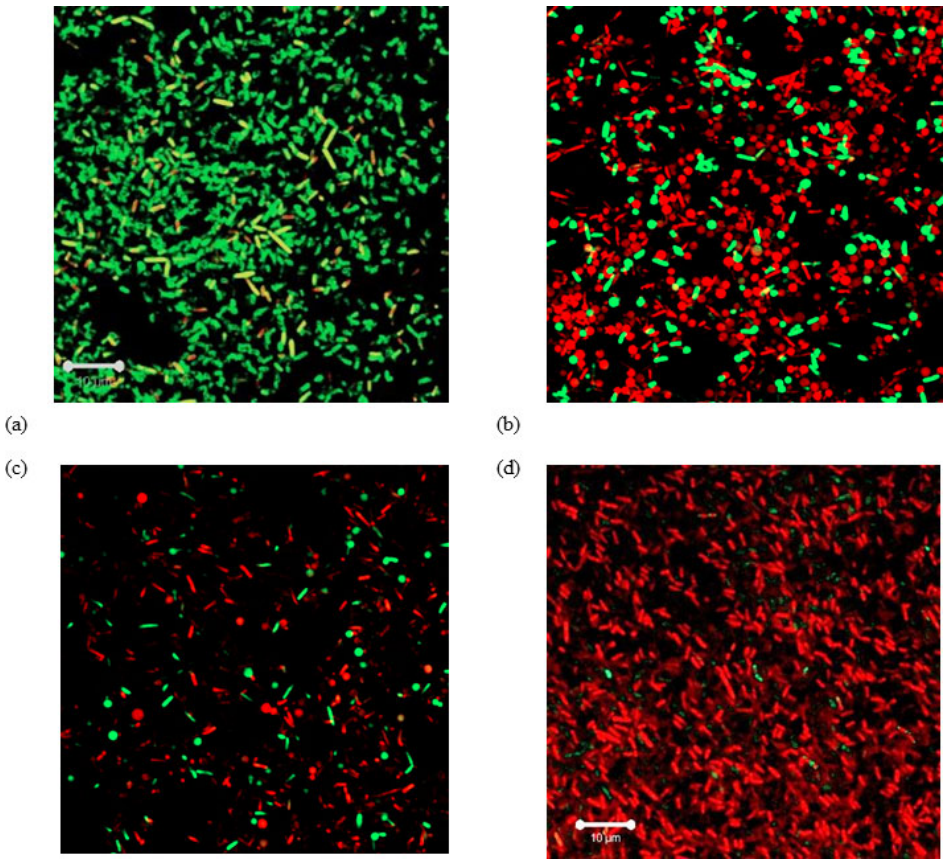

Figure 6. Live/dead assay. Representative confocal microscopy images of *E. coli* cells upon increasing exposure time to $\lambda > 320$ nm irradiation in the presence of 0.25 g L^{-1} photocatalyst. (a) Control sample without bismuth addition, (b) 0 min of treatment by irradiation with photocatalyst added, (c) 20 min of treatment with photocatalyst, (d) 40 min of treatment with photocatalyst.

Endonuclease-sensitive site assay

ESS analysis allows quantification of pyrimidine dimer formation in the DNA of a microorganism (DNA damage), as is generally caused by UVC treatment (42,43). However, in contrast to UVC and UVB, the involvement of DNA lesions in UVA solar disinfection has scarcely been investigated, with Theitler *et al.* (26) being the first to determine DNA damage by combined heat and solar irradiation.

ESS was examined here after 10 and 40 min of irradiation with and without bismuth ($\lambda > 320$ nm), using the time zero control as a blank. The results could not be averaged and it was difficult to quantify the absolute amount of ESS as levels of DNA extracted from different samples was highly variable, possibly due to the aggregation of *E. coli* cells and bismuth particles. However, a clear trend in DNA damage was evident in all experiments comparing photolysis to photocatalysis. Hence, an increase in ESS per kb DNA was observed with the addition of photocatalyst. In a representative experiment, 40 min of photocatalysis resulted in almost twice as many ESSs as after 10 min of treatment, that is 1.46 ESS kb^{-1} and 0.85 ESS kb^{-1} DNA, respectively. Photolysis alone increased the amount of ESS from 0.35 ESS kb^{-1} DNA after 10 min to 1.18 ESS kb^{-1} DNA after 40 min. These findings corresponded with the viability test results: The log inactivation increases with irradiation time and addition of photocatalyst supported the correlation between irradiation time and number of ESS per kb DNA. Thus, DNA is probably a target of photocatalytic treatment, and the severity of the damage depends on the treatment duration.

Protein release during *E. coli* inactivation

Cho *et al.* (41) suggested that proteins degrade due to reactions with disinfectants such as O_3, chlorine dioxide, free chlorine and UV irradiation. We tested whether this is the case with the bismuth photocatalyst as well. Different conditions were examined to validate the Bradford assay, because the dye in this assay—Coomassie Brilliant Blue G-250—also carries a positive charge. Experiments with bovine serum albumin (BSA) as the protein standard demonstrated that indeed, the bismuth photocatalyst affects the assay. Treated water showed 0.06 mg L^{-1} lower measurable protein when bismuth was removed by centrifugation prior to BSA addition. Interestingly, premixing the bismuth with the dye (followed by centrifugation and addition of BSA) resulted in a false increase of 1.4~1.7 mg L^{-1} in apparent protein concentration over the real concentration (see Data S2, Fig. S2a–d). Further experiments demonstrated that the bismuth photocatalyst has both light-dependent and light-independent effects—premixing of photocatalyst with BSA and centrifugation resulted in a 38% reduction in measurable protein concentration (probably due to aggregation), while the same treatment with irradiation of the mixture resulted in a 64% reduction, either due

to higher aggregation or through direct damage to the protein (see Data S2, Fig. S2e–h). These latter data were used to correct for all following experiments.

Protein release could also imply membrane damage. Here we demonstrated protein release from treated *E. coli* after either UVA or UVA/$BiOCl_{0.875}Br_{0.125}$ treatment, the release being higher when bismuth was present (after correction for the photocatalyst effect on the assay). Repeatability in the amount of protein released between the different experiments was low, probably due to the aggregation of bismuth particles and *E. coli* and/or released proteins. However, the trend of the results was consistent with an increase in supernatant protein concentration with time of irradiation (Fig. 7).

Effect of ROS scavengers

Both photosensitizers and photocatalysts bring about the photodisinfection of contaminated waters. The photodisinfection action, depending on the nature of the photosensitizer/photocatalyst, can proceed through type-I or type-II mechanism or both. Where type-I mechanism involves electron transfer from excited sensitizer to substrate molecule or oxygen yielding free radicals as HO• and superoxide ion while in type-II mechanism, energy transfer between the photosensitizer and oxygen produces singlet oxygen ($^1O_2$) (1). Photosensitizers were shown to be very effective in photodynamic killing of bacteria (44), however employing either the photocatalyst or photosensitizer as a suspension or a homogenous solution is problematic for water treatment as they must be removed from the water.

The methodologies employed to probe the modes of action of ROS in the photocatalytic degradation of organic chemicals (45) can be applied to investigate their mode of action in the inactivation of microorganisms. We investigated the contribution of two common ROS, namely HO• and singlet oxygen ($^1O_2$), to the inactivation of *E. coli* by UVA/$BiOCl_{0.875}Br_{0.125}$. In the presence of oxygen, the photosensitizer can transfer energy via type-II mechanism producing $^1O_2$, while in photocatalysis the electron–hole pair can oxidize water yielding HO• radicals, and therefore both common ROS were investigated.

To this end, inactivation in the presence of the radical scavengers L-histidine [to quench singlet oxygen (46,47)] and tert-butanol [to quench hydroxyl radicals (48,49)] added to the bulk water was followed. Neither radical scavenger had any effect on the inactivation of *E. coli*. In all cases, 40 min of photocatalytic treatment resulted in ~3.5 log inactivation. These results imply that neither HO• nor $^1O_2$ is involved in the inactivation process, and are in good agreement with a previous study which showed that different HO• scavengers present in the bulk water (terephthalic acid and tert-butanol) have no influence on the photocatalytic degradation of rhodamine B by a combination of $BiOCl_{0.875}Br_{0.125}$ and visible light irradiation (13). In a valence band of Bi^{3+}, holes formed by photoexcitation are regarded as Bi^{5+}. The standard redox potential of Bi^{5+}/Bi^{3+} is more negative than of $HO•/OH^-$. Therefore, photogenerated holes on the surface of $BiOCl_{0.875}Br_{0.125}$ are not expected to react with OH^-/H_2O to form HO•, suggesting that the inactivation of *E. coli* in the present study could be attributed mainly to a direct photo-induced inactivation over the photogenerated holes.

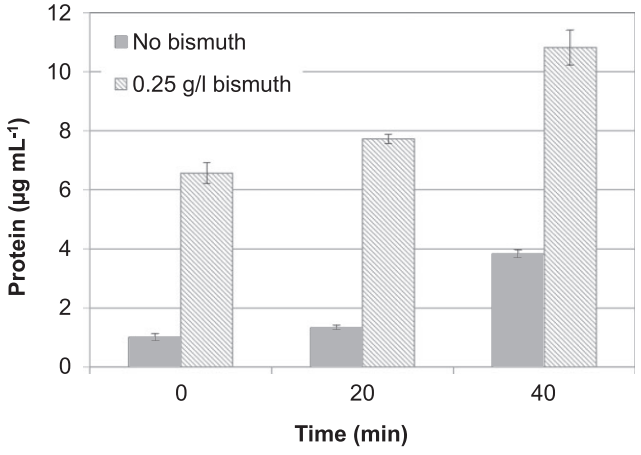

Figure 7. Protein release from treated *E. coli* cells as a function of irradiation time in the presence (0.25 g L^{-1} bismuth) or absence (no bismuth) of 0.25 g L^{-1} photocatalyst.

Formation of an electron–hole pair on the catalyst surface by a direct photocatalytic process via exposure to UV irradiation promotes an electron from its valence band to a conduction band. The possible mechanisms for bacterial inactivation at the valance band include direct and indirect oxidation:

$$h^+_{vb} + \text{Bacteria} \rightarrow \text{Bacteria}^+ (\text{direct bacteria oxidation})$$

$$h^+_{vb} + H_2O \rightarrow H^+ + HO•$$

$$HO• + \text{Bacteria} \rightarrow \text{Bacteria degradation (indirect)}$$

A high oxidation potential of the hole h^+_{vb} promotes a direct bacterial oxidation. Electron holes produced in a direct photocatalytic process require the adsorption of bacteria on the catalyst surface for its further degradation. Another mechanism is the generation of HO• radicals from water by electron holes. These deep holes (the valence band energy of $BiOCl_{0.875}Br_{0.125}$ is 3.30 eV) are efficiently reactive under UVA and are separated from the photogenerated electrons due the well-matched energy bands of the heterojunctioned photocatalyst. This notion is supported by Lester *et al.* (2014) that showed that carbamazepine (CBZ) and propranolol (PPL) have similar reaction rate constants with HO• and significantly different degradation rate by irradiated $BiOCl_{0.875}Br_{0.125}$, suggesting a none-HO•-dependent mechanism. The degradation path suggested the direct reaction of PPL with photogenerated $BiOCl_{0.875}Br_{0.125}$ holes, via an electron transfer mechanism. On the other hand, for TiO_2, photocatalytic inactivation of *E. coli* is most likely the result of HO• (both free and surface-bound) (48).

CONCLUSIONS

The use of a $BiOCl_{1-x}Br_x$-based photocatalyst (with $x > 0.87$) for the disinfection of *E. coli* in water was demonstrated. Several conclusions can be drawn regarding the inactivation efficiency and the inactivation mechanism and its limitations.

1 Bismuth oxyhalide particles caused membrane damage to *E. coli* even without irradiation, resulting in membrane permeability and protein release. Nevertheless, this damage was not extended enough to cause detectable eradication of the bacteria by enumeration.

2 UVA irradiation resulted in threefold greater rate constants of a photocatalytic reaction with bismuth photocatalyst compared with photolytic reaction alone; under UVB, the difference was less pronounced (~1.5-fold).
3 The correlation between log inactivation and Ct (where C is bismuth concentration and t is the irradiation time) exhibited a highly linear fit for UVA/$BiOCl_{0.875}Br_{0.125}$.
4 ESS assay showed that DNA is a possible target of both UVA irradiation and photocatalytic UVA/$BiOCl_{0.875}Br_{0.125}$ treatment.
5 UVB/$BiOCl_{0.875}Br_{0.125}$ inactivation of *E. coli* was not influenced by the presence of the radical scavengers tert-butanol and L-histidine added to the water, implying that HO• and $^1O_2$ are not involved in the bismuth-based photocatalytic process. The inactivation is attained mainly by the direct contribution of the photogenerated holes.
6 The photocatalytic activity is probably external to the cells and is manifested inside the cells (i.e. DNA damage) by an unknown mechanism.

Acknowledgements—This research received funding from the Israeli Science Foundation, under grant agreement 01011773 on "Novel Composite BiOCl/BiOBr and Similar Mixed Halide Heterostructures as Solar Light Driven Photocatalysts with Applications in Water Technologies."

SUPPORTING INFORMATION

Additional Supporting Information may be found in the online version of this article:

Data S1. Solar simulator absolute irradiance and *E. coli* DNA absorbance.

Data S2. Validation of Bradford assay.

Figure S1. Solar simulator absolute irradiance and *E. coli* DNA absorbance at different wavelengths.

Figure S2. Effect of bismuth treatment on measured protein concentration. For experimental details, see Data S2.

REFERENCES

1. Thandu, M., C. Comuzzi and D. Goi (2015) Phototreatment of water by organic photosensitizers and comparison with inorganic semiconductors. *Int. J. Photoenergy* **2015**, 1–22.
2. Hoffmann, M. R., S. T. Martin, W. Y. Choi and D. W. Bahnemann (1995) Environmental applications of semiconductor photocatalysis. *Chem. Rev.* **95**, 69–96.
3. Hashimoto, K., H. Irie and A. Fujishima (2005) TiO_2 photocatalysis: A historical overview and future prospects. *Jpn. J. Appl. Phys.* **44**, 8269–8285.
4. Spasiano, D., R. Marotta, S. Malato, P. Fernandez-Ibanez and I. Di Somma (2015) Solar photocatalysis: materials, reactors, some commercial, and pre-industrialized applications A comprehensive approach. *Appl. Catal. B-Environ.* **170**, 90–123.
5. Rohr, O. (2002) Bismuth – the new ecologically green metal for modern lubricating engineering. *Industr. Lubricat. Tribol.* **54**, 153–153.
6. Tang, J. W., Z. G. Zou and J. H. Ye (2004) Efficient photocatalytic decomposition of organic contaminants over $CaBi_2O_4$ under visible-light irradiation. *Angew. Chem. Int. Ed. Engl.* **43**, 4463–4466.
7. Kako, T., Z. Zou, M. Katagiri and J. Ye (2006) Decomposition of organic compounds over $NaBiO_3$ under visible light irradiation. *Chem. Mater.* **19**, 198–202.
8. Wang, C. Y., H. Zhang, F. Li and L. Y. Zhu (2010) Degradation and mineralization of bisphenol A by mesoporous Bi_2WO_6 under simulated solar light irradiation. *Environ. Sci. Technol.* **44**, 6843–6848.
9. Ren, J., W. Wang, L. Zhang, J. Chang and S. Hu (2009) Photocatalytic inactivation of bacteria by photocatalyst Bi_2WO_6 under visible light. *Catal. Commun.* **10**, 1940–1943.
10. Zhang, L. S., K. H. Wong, H. Y. Yip, C. Hu, J. C. Yu, C. Y. Chan and P. K. Wong (2010) Effective photocatalytic disinfection of *E. coli* K-12 using AgBr− Ag− Bi_2WO_6 nanojunction system irradiated by visible light: The role of diffusing hydroxyl radicals. *Environ. Sci. Technol.* **44**, 1392–1398.
11. Wang, W. J., Y. Yu, T. C. An, G. Y. Li, H. Y. Yip, J. C. Yu and P. K. Wong (2012) Visible-light-driven photocatalytic inactivation of *E. coli* K-12 by bismuth vanadate nanotubes: bactericidal performance and mechanism. *Environ. Sci. Technol.* **46**, 4599–4606.
12. Shenawi-Khalil, S., V. Uvarov, Y. Kritsman, E. Menes, I. Popov and Y. Sasson (2011) A new family of BiO(Cl x Br 1–x) visible light sensitive photocatalysts. *Catal. Commun.* **12**, 1136–1141.
13. Gnayem, H. and Y. Sasson (2013) Hierarchical nanostructured 3D flowerlike BiOCl x Br1–x semiconductors with exceptional visible light photocatalytic activity. *ACS Catal.*, **18**, 6–191.
14. Malato, S., P. Fernandez-Ibanez, M. I. Maldonado, J. Blanco and W. Gernjak (2009) Decontamination and disinfection of water by solar photocatalysis: Recent overview and trends. *Catal. Today* **147**, 1–59.
15. Avery, S. V. (2011) Molecular targets of oxidative stress. *Biochem. J.* **434**, 201–210.
16. Cabiscol, E., J. Tamarit and J. Ros (2000) Oxidative stress in bacteria and protein damage by reactive oxygen species. *Int. Microbiol.* **3**, 3–8.
17. Kielbassa, C., L. Roza and B. Epe (1997) Wavelength dependence of oxidative DNA damage induced by UV and visible light. *Carcinogenesis* **18**, 811–816.
18. Mamane, H., H. Shemer and K. G. Linden (2007) Inactivation of *E-coli*, B-subtilis spores, and MS2, T4, and T7 phage using UV/H_2O_2 advanced oxidation. *J. Hazard. Mater.* **146**, 479–486.
19. Dalrymple, O. K., E. Stefanakos, M. A. Trotz and D. Y. Goswami (2010) A review of the mechanisms and modeling of photocatalytic disinfection. *Appl. Catal. B* **98**, 27–38.
20. Cockell, C. S. (1998) Biological effects of high ultraviolet radiation on early earth—a theoretical evaluation. *J. Theor. Biol.* **193**, 717–729.
21. He, Y. Y. and D. P. Hader (2002) Reactive oxygen species and UV-B: Effect on cyanobacteria. *Photochem. Photobiol. Sci.* **1**, 729–736.
22. Jiang, Y., M. Rabbi, M. Kim, C. Ke, W. Lee, R. L. Clark, P. A. Mieczkowski and P. E. Marszalek (2009) UVA generates pyrimidine dimers in DNA directly. *Biophys. J* . **96**, 1151–1158.
23. Chong, M. N., B. Jin, C. W. K. Chow and C. Saint (2010) Recent developments in photocatalytic water treatment technology: A review. *Water Res.* **44**, 2997–3027.
24. Halliwell, B. and O. I. Aruoma (1991) DNA damage by oxygen-derived species its mechanism and measurement in mammalian systems. *FEBS Lett.* **281**, 9–19.
25. Grune, T., T. Jung, K. Merker and K. J. Davies (2004) Decreased proteolysis caused by protein aggregates, inclusion bodies, plaques, lipofuscin, ceroid, and 'aggresomes' during oxidative stress, aging, and disease. *Int. J. Biochem. Cell Biol.* **36**, 2519–2530.
26. Theitler, D. J., A. Nasser, Y. Gerchman, A. Kribus and H. Mamane (2012) Synergistic effect of heat and solar UV on DNA damage and water disinfection of *E. coli* and bacteriophage MS2. *J. Water Health* **10**, 605–618.
27. Lester, Y., D. Avisar, H. Gnayem, Y. Sasson, M. Shavit and H. Mamane (2014) Demonstrating a new BiOCl 0.875Br 0.125 photocatalyst to degrade pharmaceuticals under solar irradiation. *Water Air Soil Pollut.* **225**, 1–11.
28. Adán, C., J. Marugán, S. Obregón and G. Colón (2015) Photocatalytic activity of bismuth vanadates under UV-A and visible light irradiation: Inactivation of *Escherichia coli* vs oxidation of methanol. *Catal. Today* **240**, 93–99.
29. Boyle, M., C. Sichel, P. Fernandez-Ibanez, G. B. Arias-Quiroz, M. Iriarte-Puna, A. Mercado, E. Ubomba-Jaswa and K. G. McGuigan (2008) Bactericidal effect of solar water disinfection under real sunlight conditions. *Appl. Environ. Microbiol.* **74**, 2997–3001.

30. Ibáñez, J. A., M. I. Litter and R. A. Pizarro (2003) Photocatalytic bactericidal effect of TiO_2 on *Enterobacter cloacae*: Comparative study with other Gram (−) bacteria. *J. Photochem. Photobiol., A* **157**, 81–85.
31. Liu, H. L. and T. C. K. Yang (2003) Photocatalytic inactivation of *Escherichia coli* and *Lactobacillus helveticus* by ZnO and TiO_2 activated with ultraviolet light. *Process Biochem.* **39**, 475–481.
32. Benabbou, A. K., Z. Derriche, C. Felix, P. Lejeune and C. Guillard (2007) Photocatalytic inactivation of *Escherischia coli*: Effect of concentration of TiO_2 and microorganism, nature, and intensity of UV irradiation. *Appl. Catal. B* **76**, 257–263.
33. Chick, H. (1908) An investigation of the laws of disinfection. *Epidemiol. Infect.* **8**, 92–158.
34. Watson, H. E. (1908) A note on the variation of the rate of disinfection with change in the concentration of the disinfectant. *Epidemiol. Infect.* **8**, 536–542.
35. Cho, M., H. Chung, W. Choi and J. Yoon (2004) Linear correlation between inactivation of *E. coli* and OH radical concentration in TiO_2 photocatalytic disinfection. *Water Res.* **38**, 1069–1077.
36. Pigeot-Rémy, S., F. Simonet, D. Atlan, J. C. Lazzaroni and C. Guillard (2012) Bactericidal efficiency and mode of action: A comparative study of photochemistry and photocatalysis. *Water Res.* **46**, 3208–3218.
37. Josset, S., N. Keller, M. C. Lett, M. J. Ledoux and V. Keller (2008) Numeration methods for targeting photoactive materials in the UV-A photocatalytic removal of microorganisms. *Chem. Soc. Rev.* **37**, 744–755.
38. Carre, G., E. Hamon, S. Ennahar, M. Estner, M. C. Lett, P. Horvatovich, J. P. Gies, V. Keller, N. Keller and P. Andre (2014) TiO_2 photocatalysis damages lipids and proteins in *Escherichia coli*. *Appl. Environ. Microbiol.* **80**, 2573–2581.
39. Maness, P.-C., S. Smolinski, D. M. Blake, Z. Huang, E. J. Wolfrum and W. A. Jacoby (1999) Bactericidal activity of photocatalytic TiO_2 reaction: Toward an understanding of its killing mechanism. *Appl. Environ. Microbiol.* **65**, 4094–4098.
40. Sokmen, M., F. Candan and Z. Sumer (2001) Disinfection of *E-coli* by the Ag-TiO_2/UV system: Lipidperoxidation. *J. Photochem. Photobiol. A-Chem.* **143**, 241–244.
41. Cho, M., J. Kim, J. Y. Kim, J. Yoon and J.-H. Kim (2010) Mechanisms of *Escherichia coli* inactivation by several disinfectants. *Water Res.* **44**, 3410–3418.
42. Oguma, K., H. Katayama, H. Mitani, S. Morita, T. Hirata and S. Ohgaki (2001) Determination of pyrimidine dimers in *Escherichia coli* and *Cryptosporidium parvum* during UV light inactivation, photoreactivation, and dark repair. *Appl. Environ. Microbiol.* **67**, 4630–4637.
43. Eischeid, A. C. and K. G. Linden (2007) Efficiency of pyrimidine dimer formation in *Escherichia coli* across UV wavelengths. *J. Appl. Microbiol.* **103**, 1650–1656.
44. Huang, L., T. G. S. Denis, Y. Xuan, Y.-Y. Huang, M. Tanaka, A. Zadlo, T. Sarna and M. R. Hamblin (2012) Paradoxical potentiation of methylene blue-mediated antimicrobial photodynamic inactivation by sodium azide: Role of ambient oxygen and azide radicals. *Free Radic. Biol. Med.* **53**, 2062–2071.
45. Kim, S. and W. Choi (2002) Kinetics and mechanisms of photocatalytic degradation of (CH3) n NH4-n+($0 \leq n \leq 4$) in TiO_2 suspension: The role of OH radicals. *Environ. Sci. Technol.* **36**, 2019–2025.
46. Hara, K., S. Holland and J. Woo (2004) Effects of exogenous reactive oxygen species scavengers on the survival of *Escherichia coli* B23 during exposure to UV-A radiation. *J. Exp. Microbiol. Immunol.* **12**, 62–66.
47. Ishiyama, K., K. Nakamura, H. Ikai, T. Kanno, M. Kohno, K. Sasaki and Y. Niwano (2012) Bactericidal action of photogenerated singlet oxygen from photosensitizers used in plaque disclosing agents. *PLoS ONE* **7**, e37871.
48. Cho, M., H. Chung, W. Choi and J. Yoon (2005) Different inactivation behaviors of MS-2 phage and *Escherichia coli* in TiO_2 photocatalytic disinfection. *Appl. Environ. Microbiol.* **71**, 270–275.
49. Cho, M. and J. Yoon (2006) Enhanced bactericidal effect of O_3/H_2O_2 followed by Cl_2. *Ozone: Sci. Eng.* **28**, 335–340.
50. Gan, H., G. Zhang and H. Huang (2013) Enhanced visible-light-driven photocatalytic inactivation of *Escherichia coli* by Bi2 O2 CO3/Bi3 NbO7 composites. *J. Hazard. Mater.* **250**, 131–137.